Structures of exfoliated single layers of WS_2, MoS_2, and $MoSe_2$ in aqueous suspension

R. A. Gordon, D. Yang, E. D. Crozier, D. T. Jiang,* and R. F. Frindt†

Department of Physics, Simon Fraser University, Burnaby, British Columbia, Canada V5A 1S6

(Received 2 October 2000; revised manuscript received 19 October 2001; published 1 March 2002)

Single layers of the transition-metal dichalcogenides WS_2, MoS_2, and $MoSe_2$ were formed as aqueous suspensions by lithium intercalation and exfoliation of crystalline powders and examined by x-ray diffraction and x-ray absorption fine structure (XAFS) spectroscopy. The two-dimensional characteristics of these systems were readily apparent through the absence of any (hkl) peaks $(l \neq 0)$ and in the strong asymmetry of the $(hk0)$ peaks in the diffraction patterns. Indexing the diffraction patterns with rectangular unit cells revealed the diselenide as the most distorted from the hexagonal structures of the parent materials, with the Mo atoms forming a ''zigzag'' structure which is also corrugated perpendicular to the layers. Mo K-edge and W $L3$-edge XAFS analysis using WTe_2-related structural models enabled the determination of the short, intermediate, and long metal-metal near-neighbor distances with the shortest metal-metal distances contracted approximately 0.4 Å compared to parent reference materials. Shifts in the Mo K-absorption-edge energy in $MoSe_2$ correlated with changing Se-Se interactions. Combining the XAFS and diffraction results enabled an estimation of the layer puckering and atomic positions in three-dimensional models of the unit cells. Selenium K-edge XAFS also identified two selenium-oxygen scattering paths from water or OH^- ions coordinating the layers of exfoliated $MoSe_2$.

DOI: 10.1103/PhysRevB.65.125407 PACS number(s): 71.45.Lr, 78.70.Dm

I. INTRODUCTION

Because of their unique physical and electronic structure, the layered dichalcogenides display a variety of interesting properties and phases primarily due to their ''two-dimensional'' (2D) nature, including highly anisotropic mechanical, optical, and electrical properties.[1] Some of the systems are semiconductors and some are metals or semimetals. The metals display charge density wave transitions (CDW's) and superconductivity, and are of particular interest because of their structural and electronic similarity to the high-temperature superconductors.

Because of the weak bonding between the layers, it has been possible to exfoliate (separate into single molecular layers) a number of layered dichalcogenides, including the semiconductors MoS_2, $MoSe_2$, and WS_2 and the metals 2H-NbS_2 and 2H-TaS_2.[2,3] The semiconductors are more readily exfoliated and tend to be more stable than the metals.

To date, no structural studies have been carried out on the single-layer metals and little work on their physical properties has been done. For example, it is not known if the CDW's and superconductivity of bulk 2H-NbS_2 and 2H-TaS_2 persist in the isolated single-layer form.

In this paper, as part of an ongoing study of single-layer dichalcogenides, we report on x-ray diffraction and x-ray absorption fine structure (XAFS) studies on single layer MoS_2, $MoSe_2$, and WS_2 in suspension and unambiguously determine the structure of the isolated single layers.

The properties of single-layer MoS_2, $MoSe_2$, and WS_2 and related dichalcogenides and their layered nanocomposites have not been extensively studied to date: however, changes in structure can be expected to result in significant property changes relative to the unexfoliated bulk crystals. For example, it has been observed that single-layer MoS_2 and WS_2 in suspension do not display the interband optical absorption of the bulk semiconductors.[2] This can be attributed to a change in band structure resulting from a change from trigonal prism to octahedral coordination of S around the Mo or W atom on exfoliation.[3–5] However, in addition, as we demonstrate in this paper, there is a significant distortion of the Mo (or W) structure within the layer, from 2D hexagonal to a ''zigzag'' structure which, in addition, is corrugated perpendicular to the layer. A similar structure is seen in crystalline WTe_2 and also in Li-intercalated MoS_2 and restacked single-layer MoS_2.[6,7]

Because of the zigzag structure, we expect that single-layer MoS_2, $MoSe_2$, WS_2, etc., will display strong in-plane anisotropy in the optical constants, electrical conductivity, and susceptibility. In addition, the structure may encourage alignment of adsorbed molecules onto the single layers.

The band structures of transition-metal dichalcogenides have been discussed by Mattheiss[8] and Kertesz and Hoffmann[8] and other workers. However, as we demonstrate in this paper, single-layer MoS_2, $MoSe_2$, and WS_2 in suspension have a structure that is very different from that of a layer in the bulk crystal. Using the structures presented here, detailed calculations of the band structure for these ''two-dimensional'' single-layer dichalcogenides are now possible.

Exfoliated single layers can be restacked with organic or inorganic molecules incorporated between the layers.[7,9–13] This provides a novel approach for the synthesis and study of the properties of new layered nanocomposites.

Knowledge of the exact structure of these single layer systems is incomplete. X-ray absorption fine structure studies performed on single-layer MoS_2 and derivative nanocomposites[13–15] have revealed short, intermediate, and long Mo-Mo distances, indicating a distortion from the hexagonal parent structure. Scanning transmission microscopy (STM) on bilayer $MoS_2 \cdot 2H_2O$ (Ref. 16) and incompletely oxidized $K_x(H_2O)_yMoS_2$ (Ref. 17) have indicated in-plane unit cells related to the parent MoS_2 by either an oblique $a \times 2a$ or a rectangular $a \times \sqrt{3}a$ distortion with the suggestion

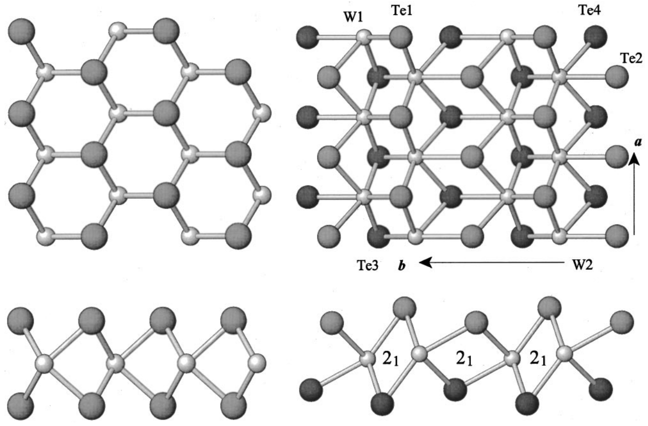

FIG. 1. Comparison of trigonal prismatic metal coordination in MoS_2 (left) and octahedral metal coordination in WTe_2 (right) single layers. Small spheres are metal atoms. Large spheres are chalcogen atoms.

of a relationship to orthorhombic WTe_2.[6,16,18] Recent electron crystallography work[7] on restacked materials have similarly indicated rectangular $a\times\sqrt{3}a$ unit cells for MoS_2 and WS_2 and produced two-dimensional structural models related to WTe_2 in plane group *pg* for the restacked layers.

Individual layers from crystalline MoS_2 and WTe_2 are compared in Fig. 1. In both structures, the metal atoms are coordinated by six nearest chalcogen neighbors with the coordination being trigonal prismatic in MoS_2 and distorted octahedral in WTe_2.[1] A displacement of the metal atom from the center of the cell in WTe_2 produces a splitting of the six nearest metal-metal distances into two short (2.85 Å), two intermediate (a axis, 3.477 Å), and two long (4.37 Å) distances. A 0.21-Å puckering of the metal layer accompanies the displacement. While in the full WTe_2 crystal structure there are two crystallographically inequivalent W sites and four inequivalent Te sites, within a single layer, the metal atoms and two pairs of chalcogen atoms (Te1, Te3 and Te2, Te4) appear to be related by a 2_I screw axis along the short axis a. The glide plane determined from the two-dimensional electron crystallography work on restacked materials[7] would be the projection of this screw axis into the plane if the layers are structurally related to WTe_2.

Layered nanocomposite materials are prepared by restacking exfoliated single layers. To understand fully the restacking process, what is ultimately needed are accurate structural models of the layers in suspension. Both x-ray diffraction and XAFS can be done on samples in aqueous suspension. The strongly two-dimensional nature of the diffraction patterns for these systems makes complete analysis of the unit cell contents by diffraction impossible, since ‘‘two-dimensional’’ diffraction from randomly oriented single layers provides little information on atomic positions perpendicular to the plane of the layers. XAFS can provide distances between absorbing and scattering atoms in the layers. By combining diffraction results of higher resolution than previously reported[2,19] for WS_2 and MoS_2, and new data on $MoSe_2$, with XAFS data on these exfoliated layer systems, and some elementary geometry,[16] we have obtained three-dimensional models of the randomly oriented single layers in suspension. To our knowledge, this is the first direct and unambiguous structure determination of randomly oriented monomolecular layers in suspension.

TABLE I. Summary of lithium intercalation ($y\geqslant 1$) conditions in preparation of the exfoliated layers in 2.5 M *n*-butyl lithium in hexane.

Li_yMX_2	Temperature and duration
Li_yWS_2	100 °C, 18 h
Li_yMoS_2	20 °C, 18 h or 100 °C, 1 h
Li_yMoSe_2	20 °C, 2 weeks or 60 °C, 18 h

II. EXPERIMENT

Exfoliated samples of the disulphides were prepared by lithium intercalation and extraction as per the literature[2] by reaction with 2.5 M *n*-butyl lithium in hexane (under argon) and subsequent reaction and repeated washing with distilled, de-ionized water until a $p\mathrm{H}\sim 7$ was obtained. For complete exfoliation, preparation of Li_yMX_2 with $y\geqslant 1$ was necessary. The preparation of exfoliated $MoSe_2$ has not been previously reported, but is straightforward. After lithium intercalation of the 2H (trigonal prismatic) parent material and addition of distilled water, exfoliated layers are immediately obtained. Washing with distilled water is still performed to reduce the pH to ~7. Table I summarizes the conditions used to perform the lithium intercalation. The exfoliated layers are sheets one molecular layer thick (6 Å) and are typically 0.1–1μm in extent. X-ray diffraction measurements were made using a Siemens model D5000 diffractometer (Cu $K\alpha$ radiation) on moist exfoliated slurry which was approximately 5% MX_2/95% H_2O by weight and sealed under thin kapton sheet. Note that the single layers in suspension are randomly oriented.

X-ray absorption measurements were made at the PNC-CAT undulator beamline, Sector 20, Advanced Photon Source.[20] Distilled, de-ionized water was added to moist paste of the exfoliated materials and sealed in plastic bags. The material was allowed to settle in the bag and the bag clamped to give a region of uniform thickness. Uniformity was also checked by examining the image of the transmitted beam with a single-crystal phosphor. Powdered binary dichalcogenide samples (Aldrich) were prepared on transparent tape and examined by XAFS for reference. Sample containers (tape or bag) were oriented at an angle between 30° and 45° to the polarization vector of the synchrotron x-ray beam in case of preferred orientation of the layers relative to the container surfaces. Exfoliated $MoSe_2$ was also applied to tape and allowed to dry while being examined in the synchrotron x-ray beam. This sample will be referred to as ‘‘restacked’’ below.

A Si(111) double-crystal monochromator, detuned to 60% to reduce higher harmonics, was used to provide monochromatic x rays. Attenuation of the x-ray beam with aluminum was necessary to prevent bubble formation from water disassociation. XAFS data were collected in fluorescence and

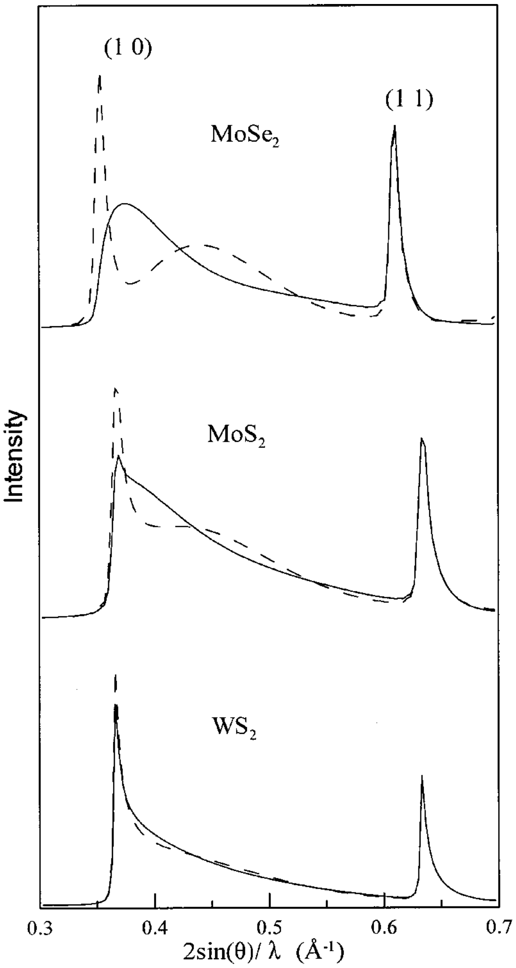

FIG. 2. Effects of changing coordination and scattering contrast on simulated diffraction patterns of hexagonal randomly oriented WS_2, MoS_2, and $MoSe_2$ single layers. Solid lines correspond to octahedral metal coordination by chalcogen atoms, and dashed lines are for trigonal prismatic coordination.

transmission modes using ionization chambers filled with helium (transmission) or argon (fluorescence) gas.

III. RESULTS AND DISCUSSION

A. Diffraction data

Before analyzing the diffraction data, the effects of the change in metal coordination from trigonal prismatic to octahedral were considered. While this change is accepted for the disulphides in the literature,[2,4,5] its effects have not been as clearly demonstrated for single layers. Figure 2 displays calculated results of the effect of the changes in coordination (trigonal prism to octahedral) and contrast in atomic scattering (difference in atomic number) for model trigonal prismatic and octahedral hexagonal single layers of WS_2, MoS_2, and $MoSe_2$. The calculated diffraction patterns in Figs. 2 and 10 were obtained using the Debye formula, described in detail in Refs. 19 and 21. In the Debye formula simulation, the positions of the atoms in the unit cell, the atomic form factors, and the sample size are the model-dependent parameters. Note that the calculated patterns in Fig. 2 are for scattering from randomly oriented single molecular layers and the standard technique used to determine structure in 3D is not available for randomly oriented 2D systems. A strong dependence of peak shape on scattering contrast is evident for the peak near 0.37 Å^{-1}. For the model tungsten compound, the scattering is dominated by the higher atomic number of W over that of S and the effect of coordination on peak shape is negligible. Differences in the peak shape are more pronounced for MoS_2. For the $MoSe_2$ simulations, where the scattering contributions from Mo and Se to the structure factor are comparable, the peak shape shows dramatic differences depending on coordination. Where the trigonal prismatic coordination would have a sharp primary peak and broad secondary feature above the peak, the octahedral coordination results in a more rounded single peak with a broad tail. Evidence of exfoliated $MoSe_2$ transforming from trigonal to octahedral metal coordination will therefore be apparent by the presence of such a broad asymmetric diffraction peak near 0.37 Å^{-1}.

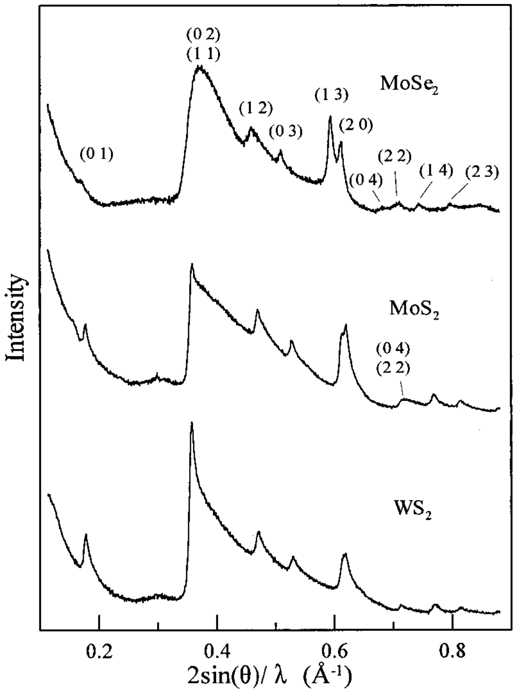

FIG. 3. Intensity of diffraction patterns as functions of 2 sin θ/λ for $MoSe_2$, MoS_2, and WS_2 single-layer aqueous suspension.

Figure 3 shows the x-ray diffraction patterns for the exfoliated suspensions. For Figs. 2, 3, and 10 note that $2\sin\theta/\lambda = 1/d = S/2\pi$, where d is the plane spacing and S is the scattering vector. A water background signal has been subtracted, with a remnant evident at about 0.3 Å^{-1}. The two-dimensional nature of the patterns in Fig. 3 is evident in the asymmetry of the peaks[21] and the ability to index the patterns with only two indices. Assignment of indices to the peaks is based on a rectangular cell related to WTe_2. The assignment of lattice directions a and b were chosen to be consistent with recent work on WTe_2 in space group $Pmm2_1$.[18] Lattice constants for the single-layer materials were determined by comparison of peak intensities and positions between the measured patterns and a calculated

TABLE II. Summary of lattice constants and deviation from hexagonal symmetry for exfoliated WS_2, MoS_2, and $MoSe_2$. In-plane constants for WTe_2 are provided for comparison from Mar *et al.* (Ref. 17). For a metrically hexagonal system, $\sqrt{3}\,a/b$ would equal 1.

MX_2	a (Å)	b (Å)	$\sqrt{3}\,a/b$
WS_2	3.23(1)	5.66(2)	0.988(7)
MoS_2	3.22(1)	5.68(2)	0.982(7)
$MoSe_2$	3.27(1)	5.90(2)	0.960(6)
WTe_2	3.477	6.249	0.964

model pattern using a layer size of 30×30 unit cells and random orientation of the layers.[21] Note that the model layer size corresponds to the coherence length or the flatness of diffraction regions of the actual molecular layers. The lattice data are given in Table II. It was not possible to obtain diffraction data on the freshly restacked $MoSe_2$ and results comparable to exfoliated MoS_2 are assumed.

Indexing with the rectangular cells leads to a deviation in the ratio b/a from the expected value of $\sqrt{3}$ for a hexagonal system (Table II), with WS_2 the least distorted and $MoSe_2$ the most. For the diselenide, the distortion from hexagonal is quite evident in the splitting of the (13) and (20) peaks when compared to the disulphides. These peaks provide strong evidence supporting the rectangular cell for $MoSe_2$ in particular. The resolution of the (13) peak for exfoliated $MoSe_2$ enables determination of the angle between the a and b axes to be 90.0(3)°. The broad, rounded, asymmetric shape of the overlapping (02) and (11) peaks for $MoSe_2$ is consistent with the change from trigonal prismatic to octahedral metal coordination. The 4% deviation of single-layer $MoSe_2$ from hexagonal is larger than that for crystalline WTe_2 (3.6%). The distortion in the exfoliated disulphides (Table II) is in contrast to the restacked disulphides where the ratio of the lattice constants is $\sqrt{3}$ (restacked WS_2 $a=3.21$ Å, MoS_2 $a=3.16$ Å).[7] The values of the a lattice parameters reported here are also larger than for the restacked materials—by 1% for WS_2 and by 2% for MoS_2. A contraction of the disulphides on restacking may account for this.

The diffraction patterns in Fig. 3 also provide the information on distortion within the unit cell. For a 2D centered rectangular structure, the structure factor calculations show that only (20), (40),... and (02), (04),... type peaks are observed. The fact that (01) and (03) peaks show up strongly in Fig. 3 demonstrates that the central metal atom of the rectangular cell has moved in the **b**-axis direction. Similarly, the absence of (10) and (30) peaks in Fig. 3 shows that there is no distortion of the central metal atom in the **a** direction (computer simulation shows that any distortion greater than 0.02 Å would be detectable). Note that single-layer diffraction is insensitive to the atomic position perpendicular to the layers.

B. XAFS data

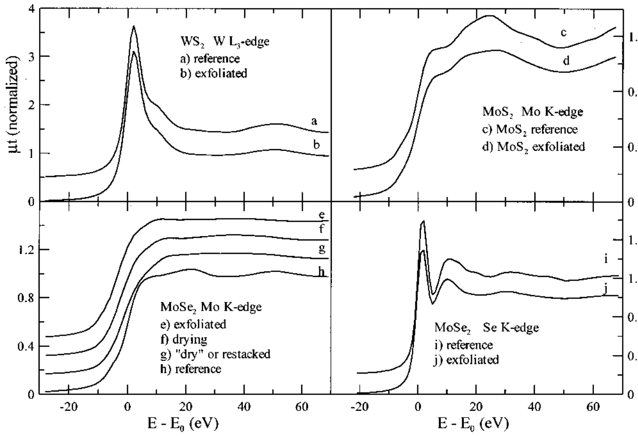

FIG. 4. X-ray near-edge spectra for reference and aqueous single-layer WS_2, MoS_2, and $MoSe_2$ compounds. Spectra have been offset vertically for clarity. Spectrum (f) was taken while the restacked sample was drying.

X-ray absorption near-edge structure (XANES) data for the samples and reference compounds are given in Fig. 4. Molybdenum data were taken in fluorescence mode while the tungsten and selenium data were taken in transmission. For the binary disulphides, no shift in edge energy (WS_2 W L_3 10 202 eV; MoS_2 Mo K 20009.1 eV), determined from the first inflection point, is apparent. For the diselenide, the molybdenum K edge for the exfoliated material is shifted 3 eV below that of the reference material ($E_0=20\,008.3$ eV) and this shift decreases as the exfoliated material dries and restacks. The Se K-edge XANES does not exhibit a shift between reference ($E_0=12\,659$ eV) and exfoliated samples.

The possibility of a residual negative charge on the exfoliated layers[7,13,22] has been considered. Since the estimated residual charge ($0.15–0.25e^-$/metal atom) is small and the step resolution of the XANES moderate at 1 eV, the lack of an observable edge shift for the sulphides does not rule out the existence of residual charge. That the more-distorted $MoSe_2$ species does exhibit an edge shift is curious, particularly since the shift to lower energy (lower oxidation state) decreases as the material dries and restacks. If this shift is

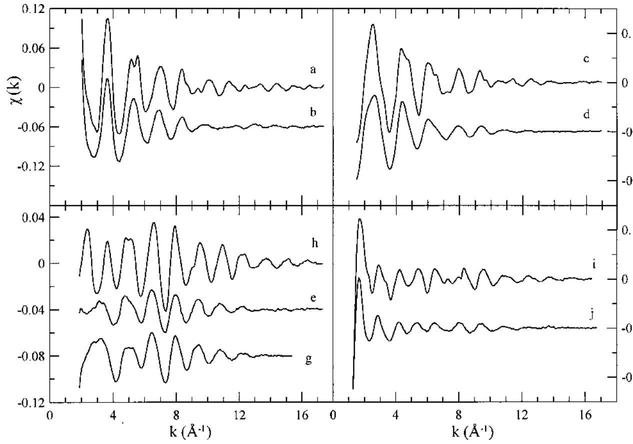

FIG. 5. XAFS interference functions $\chi(k)$ for reference and single-layer WS_2, MoS_2, and $MoSe_2$ compounds. Labeling of $\chi(k)$'s are as in Fig. 4. Spectra have been offset vertically for clarity.

TABLE III. Summary of fit values for the nearest metal-chalcogen and three metal-metal scattering for reference powder and aqueous layer extended XAFS on WS_2, MoS_2, and $MoSe_2$ for three fitting cases: single ΔE_0 (1), separate ΔE_0's (2), and separate ΔE_0's with R_{M2} constrained by diffraction (3). Statistical errors listed in parentheses were obtained from the values that doubled the minimum residual sum of squares. Systematic errors were obtained by comparison with crystalline data. Reference selenium K-edge data are also given (Se-ref.) as are fit values for restacked $MoSe_2$.

MX_2	6 at R_X (Å)	σ_X^2 (10^{-4} Å^2)	2 at R_{M1} (Å)	σ_{M1}^2 (10^{-4} Å^2)	2 at R_{M2} (Å)	σ_{M2}^2 (10^{-4} Å^2)	2 at R_{M3} (Å)	σ_{M3}^2 (10^{-4} Å^2)	ΔE_{0X} (eV)	ΔE_{0M} (eV)	res.[a] (%)
WS_2 (crystal)	2.405				6 at 3.153						
WS_2 (ref.)	2.403(4)	26(2)			3.150(6)	41(4)			5.6(6)	5.6	2.7
WS_2 (exfol.1)	2.417(2)	58(4)	2.737(3)	37(3)	3.22(2)	128(30)	3.81(2)	61(9)	4.2(3)	4.2	0.8
WS_2 (exfol.2, 3)	2.417(3)	59(2)	2.738(5)	37(3)	3.23(2)	117(20)	3.81(2)	65(12)	4.2(3)	4.6(8)	1.1
MoS_2 (crystal)	2.418				6 at 3.160						
MoS_2 (ref.)	2.397(5)	22(3)			3.152(7)	49(4)			2.3(6)	2.3	1.8
MoS_2 (exfol.1)	2.406(3)	54(2)	2.753(6)	60(4)	3.147(9)	73(7)	3.77(2)	57(20)	1.5(3)	1.5	0.9
MoS_2 (exfol.2)	2.402(3)	47(2)	2.788(5)	51(4)	3.20(1)	68(8)	3.808(16)	61(10)	1.3(4)	8.4(6)	0.3
MoS_2 (exfol.3)	2.402(5)	46(2)	2.799(4)	47(3)	3.220(7)	65(6)	3.82(1)	63(13)	1.3(8)	10.5(5)	0.6
$MoSe_2$ (crystal)	2.527				6 at 3.289						
$MoSe_2$ (Mo-ref.)	2.519(3)	27(2)			3.283(8)	59(5)			2.3(6)	2.3	1.9
$MoSe_2$ (Se-ref.)	2.521(3)	17(2)			3.285(12)	77(30)			5.1(5)	5.1	1.6
$MoSe_2$ (exfol.1)	2.528(2)	66(2)	2.761(8)	77(7)	3.206(14)	143(15)	4.038(13)	63(10)	−0.5(2)	−0.5	0.6
$MoSe_2$ (exfol.2)	2.525(2)	62(2)	2.788(4)	75(6)	3.24(2)	156(25)	4.06(2)	67(9)	−0.6(2)	2.4(10)	0.6
$MoSe_2$ (exfol.3)	2.522(2)	60(1)	2.799(6)	64(4)	3.270(15)	103(30)	4.045(15)	97(20)	−0.8(2)	3.8(6)	0.6
$MoSe_2$ (restck.3)	2.520(2)	59(1)	2.817(6)	65(5)	3.270(10)	88(10)	3.954(16)	62(17)	−0.0(2)	5.5(6)	0.9

[a]

$$\text{res.}(\%) = \frac{\Sigma|y_{\text{expt}}(i) - y_{\text{calc}}(i)|}{\Sigma|y_{\text{expt}}(i)|} \times 100.$$

due to a residual charge on the layers, then the charge would have to be transferred to species located between the layers on drying and restacking. If the shift is structural in origin, then the exfoliated and restacked structures should have a distinct difference in some feature that would cause a change in electron density on the molybdenum. While we are unable to rule out residual negative charge loss as a contributing factor, arguments in favor of a structural origin for the XANES shifts appear in Sec. III C below.

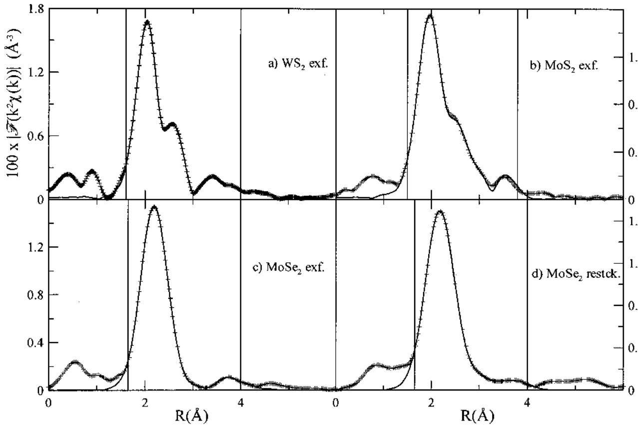

FIG. 6. Comparison of fits with the magnitudes of the k^2 Fourier transforms of the XAFS $\chi(k)$'s for the metals in single layers of (a) WS_2, (b) MoS_2, (c) $MoSe_2$, and (d) restacked $MoSe_2$ (air dried). Vertical bars indicate the regions over which the data were fit.

Extended XAFS interference functions $\chi(k)$ (Fig. 5) were extracted from the absorption data using polynomial background removal, normalization to edge jump, and a McMaster correction.[23] Fourier transforms to R space were done using k^2 weighting and a 10% Gaussian window over a range using zero crossings of $\chi(k)$ between 3–4 Å^{-1} and 13.5–15 Å^{-1}, depending on the sample. Data were fit in R space between 1.6 Å and approximately 4 Å, using models generated by the computer program FEFF7,[24] in the program WINXAS,[25] with no polarization dependence. Fits were done by iteration: fit, revise model, and refit. Since there is more than one crystallographic site for Se, the single-layer selenium data could be fit only for an average selenium atom and only with the inclusion of additional Se-O scattering paths due to the water or OH^- ions coordinating the layers.[22] Selenium-edge-fit results will be considered after the metal edges.

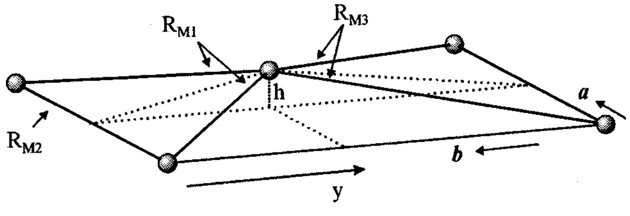

FIG. 7. Geometry for determining the out-of-plane puckering of the metal atoms for the single layers.

TABLE IV. Fractional coordinates for atoms within a single layer unit cell of WS_2, MoS_2, and $MoSe_2$ (exfoliated and restacked) obtained from best-fit XAFS distances and lattice parameters from diffraction. Errors reported are half the range obtained from positions at the maximum and minimum puckering. Positions are for half the atoms in the unit cell. Remaining atoms can be found from the transformation $(x,y,z)\Rightarrow(x+1/2,-y,-z)$.

Atom	x	y	z
WS_2, $a=3.23$ Å, $b=5.66$ Å, "c"$=6.162$ Å			
W	0	$-0.1952(5)$	0.007(12)
S1	0	0.092(17)	$-0.283(4)$
S2	0	0.428(7)	0.192(3)
MoS_2, $a=3.22$ Å, $b=5.68$ Å, "c"$=6.147$ Å			
Mo	0	$-0.1974(5)$	0.037(8)
S1	0	0.037(14)	$-0.2920(8)$
S2	0	0.407(5)	0.185(5)
$MoSe_2$, $a=3.27$ Å, $b=5.90$ Å, "c"$=6.464$ Å			
exfoliated:			
Mo	0	$-0.189(1)$	0.035(7)
Se1	0	0.036(14)	$-0.2984(10)$
Se2	0	0.414(4)	0.181(5)
restacked:			
Mo	0	$-0.1943(6)$	0.000(16)
Se1	0	0.099(14)	$-0.285(4)$
Se2	0	0.437(6)	0.199(3)

Because of the in-plane 2 screw axis, the two distinct tungsten crystallographic sites in WTe_2 (Ref. 18) are sufficiently similar in their environments (number, type, and distance of atoms) to permit treating them as equivalent by XAFS over distances out to 4.5 Å. The assumption implicit in fitting our data to a WTe_2-based model is that this also holds for the exfoliated layers. For the reference compounds[26,27] and the exfoliated samples, coordination numbers were fixed according to the crystalline or WTe_2-based structural models used, respectively. For the shifts in edge energy (ΔE_0), several different treatments were considered necessary. In standard methods, ΔE_0 is determined by fixing the distances in a reference compound to the crystallographic values and varying ΔE_0 to obtain the best fit. In doing so with the molybdenum reference compounds in this work, the fits were visibly poor with residuals more than a factor of 3 worse than when the following methods were considered.

A single shift based on reference materials has been used[13] in conjunction with FEFF. Individual shifts have also been used, but not with FEFF.[14] Correlations between the shift and R values are always a concern.[14] The change in metal environment between the reference trigonal prismatic MoS_2 structure type and the octahedral, distorted structures may invalidate transferring the shift from reference to single-layer data. The strong structural and hence electronic anisotropy in the single layers may also cause problems in FEFF calculations and may result in an anisotropic ΔE_0. Since the metal-metal interactions are largely in plane in these layer materials and the metal-chalcogen interactions out of plane, separating ΔE_0 into in-plane and out-of-plane values may allow for any anisotropy. In compromising between these concerns, we treated the fits in three ways: with a single ΔE_0 allowed to vary, with separate ΔE_0 values for *M-M* and *M-X* interactions, and with separate shifts, but the second metal-metal distance constrained to the diffraction value determined by the *a* lattice constant. Analysis of the restacked $MoSe_2$ data involved using the *a* lattice constant for the exfoliated diselenide. All other parameters (scaling S_0^2, distances $\{R_j\}$, and Debye-Waller parameters $\{\sigma_j^2\}$) were allowed to vary when fitting the sample data.

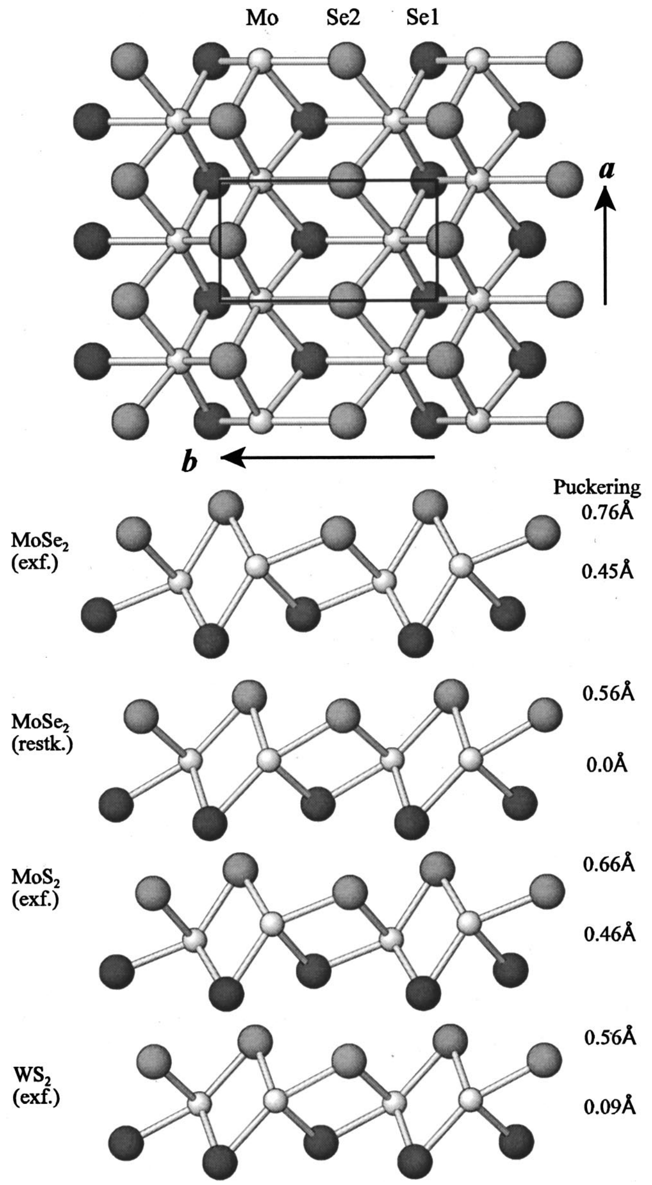

FIG. 8. Structural representations for (a) exfoliated $MoSe_2$ single-layer model viewed perpendicular to the layer and (b) single-layer $MoSe_2$ (exfoliated), $MoSe_2$ (restacked), MoS_2, and WS_2 viewed along the *a* axis. Small, white spheres are metal atoms. Larger medium and dark gray spheres are chalcogens above and below the plane, respectively.

Table III summarizes the metal-scatterer distances obtained from the fits for the nearest metal-chalcogen and

TABLE V. Comparison of model selenium to neighbor distances with XAFS Se *K*-edge diffraction-constrained (3.27 Å constrained) fit results for an average selenium in exfoliated $MoSe_2$. Two Se-O scattering paths were also fit.

Scattering path	Model Distances (Å) Se1	Model Distances (Å) Se2	Fit (Å) Se-avg.
Se-Mo	2.528	2.528	2.529(3)
Se2-Se2		3.03	2.980(2)
Se1-Se2	3.209	3.209	3.121(6)
Se-Se	3.270	3.270	3.270(5)
Se2-Mo		3.681	3.586(4)
Se1-Se2	3.710	3.710	3.778(8)
Se1-Se2	3.820	3.820	3.92(1)

metal-metal distances. Figure 6 compares the fits with the Fourier transformed data for the aqueous single-layer samples for the diffraction-constrained case. Best results were obtained for WS_2, where the difference in atomic number (Z) is the highest. The MoS_2 transform resembles that for earlier data on MoS_2 layers separated by a water bilayer in Fig. 3 (curve *C*) of Ref. 12 and may indicate some partial restacking of the sample. Two additional W-S scattering paths could also be fit in the WS_2 data, yielding values of R_{X2} of 3.58(1) Å and R_{X3} of 4.04(5) Å. Similar paths in the other samples gave weak contributions to the transforms and could not be fit reliably. The absence or presence of these weak contributions in the fits affected the position of the third metal-metal distances by 0.01–0.02 Å. The numbers in Table III are the results from including these extra *M-X* paths. Previous fits to XAFS data on MoS_2-related species fit only a nearest metal-chalcogen path.[10,12] Generally, though, lower confidence is had in the MoS_2 and $MoSe_2$ systems, where the difference in Z is lower and the features beyond the first peak in the transforms are weaker.

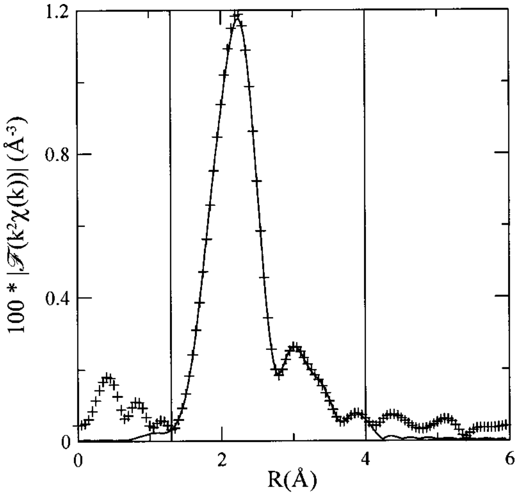

FIG. 9. Comparison of the *R*-space fit with the magnitude of the k^2 Fourier transform of the selenium *K*-edge XAFS $\chi(k)$ for exfoliated $MoSe_2$. Vertical bars indicate the region over which the data were fit.

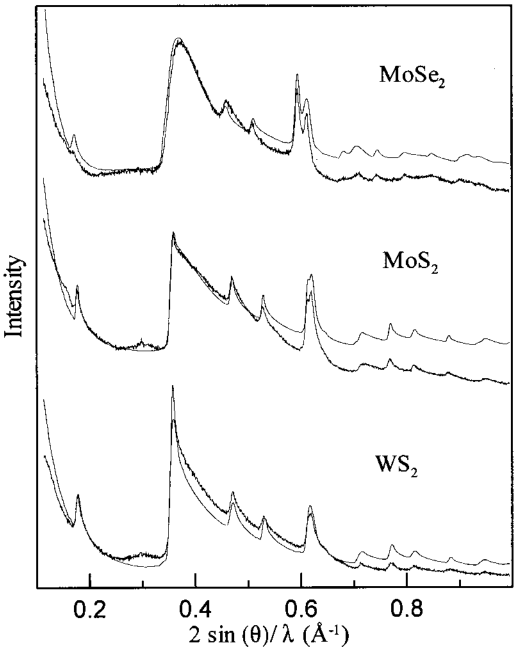

FIG. 10. Comparison of the x-ray diffraction data with simulations based on the atomic positions given in Table IV for exfoliated WS_2, MoS_2, and $MoSe_2$ suspensions. Light lines correspond to the simulations.

From Table III, the correlation between the R values and the E_0 shifts is quite apparent. Treating the data with only a single ΔE_0 resulted in smaller metal-metal distances since the shift for the nearest metal-chalcogen scattering tends to dominate. Metal-metal values were larger for the second case, where separate shifts were permitted to float, and larger still in the third case, where the second metal-metal distance was constrained to be the *a* lattice constant. For further work in determining atomic positions in the unit cell, the constrained fit results were used.

C. Geometry, XAFS, and diffraction combined

The positions of the metal atoms in a WTe_2-related unit cell can be readily obtained from the geometry of Fig. 7. After determining, from Pythagorean calculations, the lengths of the bisectors that connect the out-of-plane metal atom to the midpoint of the *a* axis, the cosine of the out-of-plane angle was determined. The puckering *h* and fractional coordinate along the *b* axis, *y*, followed. The values obtained for the exfoliated layers and restacked $MoSe_2$ are WS_2—$h=0.09(15)$ Å, $y=0.391(1)$; MoS_2—$h=0.46(5)$ Å, $y=0.395(1)$; $MoSe_2$ (exfol)—$h=0.45(9)$ Å, $y=0.378(1)$; and $MoSe_2$ (restck.)—$h=0.0(2)$, $y=0.3886(12)$. Interestingly, the restacked $MoSe_2$ layers appear to have no puckering of the metal atoms, but retain the octahedral chalcogen coordination of the metals. Because of the large error bar, however, a small puckering is possible.

For the three-dimensional models, the chalcogen positions were located at the fit nearest-neighbor distance from the metal atoms. Corrections of 0.02 and 0.008 Å were added to the Mo-S and Mo-Se distances, respectively, based on the offset of the reference from the crystal value. Choosing half the *c* axes of the 2H-MX_2 structured parents to give out-of-plane scaling for fractional *z* coordinates leads to the model unit-cell atomic positions listed in Table IV for the exfoliated layers (and restacked $MoSe_2$). Although in WTe_2 there are two metal and four chalcogen atomic (and crystallographic) positions in the unit cell, the 2_1 screw axis within the layer simplifies this to the one metal and two chalcogens reported in Table IV. The other atom positions in the unit cell can be obtained by the transformation $(x,y,z) \Rightarrow (x+\frac{1}{2},-y,-z)$. A representation of the exfoliated $MoSe_2$ layer is given in Fig. 8. Additional metal-chalcogen distances in WS_2 fit at 3.58(1) and 4.04(5) Å, while the corresponding model values are 3.70(7) and 4.03(1) Å. Comparable paths in exfoliated MoS_2, at 3.66(1) and 3.85(5) Å, do not compare favorably with model values of 3.55(5) and 4.03(1) Å. Likewise, similar *M*-*X* paths in exfoliated $MoSe_2$, at 3.53(1) and 4.10(2) Å, are inconsistent with 3.68(5) and 4.13(1) Å predicted by the model derived from the metal-metal paths and the diffraction values for the lattice constants. These paths are not strong contributions to the XAFS and may not have been fit well. Inaccuracies in the models may also exist.

The selenium *K*-edge XAFS $\chi(k)$ for the exfoliated $MoSe_2$ was transformed over the range 2.64–14.2 $Å^{-1}$ with k^2 weighting and 10% Gaussian window similar to the metal edges. The fit in *R* space was done over the region 1.3–4.0 Å and was based on the model determined from the Mo edge. A single ΔE_0 was used, and one Se-Se distance was constrained to be the *a* lattice constant from diffraction. The distances obtained from the fit are compared to those predicted by the model in Table V. Two additional Se-O backscattering paths at 2.02(1) and 2.30(2) Å were necessary for the fit. A comparison of fit with transformed data is given in Fig. 9. Fit and model values are not consistent within the errors (errors from doubling the minimum residual sum of squares as per Table III) determined from the XAFS analysis.

Comparisons of the single-layer suspension diffraction data of Fig. 3 with simulated diffraction patterns based on the positions in Table IV are given in Fig. 10.

In comparing the structures of exfoliated and restacked $MoSe_2$, it can be seen that the decrease in puckering on restacking is not accompanied by a large change in the nearest metal-metal distance. The model for the exfoliated layer does possess a chain of short (across intralayer) Se2-Se2 contacts at 3.03 Å (2.98 Å from the Se *K*-edge analysis) which increases to 3.14 Å on restacking. Both distances are less than in the parent 2H-$MoSe_2$ (3.335 Å intralayer), but considerably larger than in elemental Se (2.32 Å). The disulphide models also possess moderately short S-S distances: 2.97 and 2.98 Å, respectively, for the tungsten and molybdenum materials. These distances are also less than in their respective parent compounds, but to a lesser extent than in the exfoliated diselenide. Strong Te-Te interactions are present in WTe_2,[18] so chalcogen-chalcogen interactions in the exfoliated layers can also be expected. In particular, increased Se-Se interactions appear to be driving the larger distortion for $MoSe_2$. An increase in Se-Se interactions (bonding) would result in electron transfer back to the Mo, lowering the effective oxidation state of the Mo, and would cause the observed decrease in the absorption onset energy evident in the XANES of Fig. 4.

IV. CONCLUSIONS

Three-dimensional models of the structures of single layers of WS_2, MoS_2, and $MoSe_2$ in suspension have been obtained by combining x-ray absorption fine structure studies of the W *L*3, Mo *K*, and Se *K* edges with x-ray diffraction results. The diffraction data show that the single layers have a two-dimensional rectangular unit cell rather than the hexagonal cell of the bulk structure. The layers exhibit short, intermediate, and long metal-metal distances and octahedral chalcogen nearest-neighbor coordination consistent with a ‘‘zig zag’’ distortion of the metal which is also corrugated perpendicular to the layers. The distortion is largest in the diselenide due to increased Se-Se interactions in addition to metal-metal bonding. Two Se-O distances attributed to water or OH ions also were identified coordinating the $MoSe_2$ layers at 2.02(1) and 2.30(2) Å.

ACKNOWLEDGMENTS

This work was supported by Natural Sciences and Engineering Research Council of Canada through operating grants and a major facilities access grant. Experiments at the PNC-CAT beamline, Advanced Photon Source, Argonne National Laboratory, are also supported by the U.S. Department of Energy, Basic Energy Sciences under Contract Nos. W-31-109-Eng-38 (APS) and DE-FG03-97ER45628 (PNC-CAT). We would also like to thank M. Newville and J. O. Cross for discussions on FEFF, ΔE_0, and anisotropy.

---

*Present address: Canadian Light Source, Saskatoon, SK S7N 5C6.

†Corresponding author.

[1] A. A. Balchin, in *Crystallography and Crystal Chemistry of Materials with Layered Structures*, edited by F. Levy (Reidel, Dordrecht, 1976), Chap. 1.

[2] P. Joensen, R. F. Frindt, and S. R. Morrison, Mater. Res. Bull. **21**, 457 (1986); D. Yang and R. F. Frindt, J. Phys. Chem. Solids **57**, 1113 (1996).

[3] M. B. Dines, Mater. Res. Bull. **10**, 287 (1975); D. W. Murphy and G. W. Hull, Jr., J. Chem. Phys. **62**, 973 (1975); C. Liu, O. Singh, P. Joensen, A. E. Curzon, and R. F. Frindt, Thin Solid Films **113**, 165 (1984).

[4] H.-L. Tsai, J. Heising, J. L. Schindler, C. R. Kannewurf, and M. Kanatzidis, Chem. Mater. **9**, 879 (1997).

[5] M. A. Py and R. R. Haering, Can. J. Phys. **61**, 76 (1983).

[6] B. E. Brown, Acta Crystallogr. **20**, 268 (1966).

[7] J. Heising and M. G. Kanatzidis, J. Am. Chem. Soc. **121**, 11 720 (1999); **121**, 638 (1999).

[8] L. R. Mattheiss, Phys. Rev. B **8**, 3719 (1973); M. Kertesz and R. Hoffmann, J. Am. Chem. Soc. **106**, 3453 (1984). See also references cited in Ref. 7.

[9] W. M. R. Divigalpitiya, R. F. Frindt, and S. R. Morrison, Science **246**, 369 (1989).

[10] R. Bissessur, J. L. Schindler, C. R. Kannenwurf, and M. Kanatzi-

dis, Mol. Cryst. Liq. Cryst. **245**, 249 (1994).

[11] R. Bissessur, J. Heising, W. Hirpo, and M. Kanatzidis, Chem. Mater. **8**, 318 (1996).

[12] Y. Taguchi, R. Kimura, R. Azumi, H. Tachibana, N. Koshizaki, M. Shimomura, N. Momozawa, H. Sakai, M. Abe, and M. Matsumoto, Langmuir **14**, 6550 (1998).

[13] K. E. Dungey, M. D. Curtis, and J. E. Penner-Hahn, Chem. Mater. **10**, 2152 (1998).

[14] P. Joensen, E. D. Crozier, N. Alberding, and R. F. Frindt, J. Phys. C **20**, 4043 (1987).

[15] Y. V. Zubavichus, A. S. Golub, Y. N. Novikov, Y. L. Slovokhotov, A. N. Nesmeyanov, P. J. Schilling, and R. C. Tittsworth, J. Phys. IV **7**, C2-1057 (1997).

[16] X. R. Qin, D. Yang, R. F. Frindt, and J. C. Irwin, Phys. Rev. B **44**, 3490 (1991).

[17] F. Wypych, Th. Weber, and R. Prins, Chem. Mater. **10**, 723 (1998).

[18] A. Mar, S. Jobic, and J. A. Ibers, J. Am. Chem. Soc. **114**, 8963 (1992).

[19] D. Yang, S. Jiménez Sandoval, W. M. R. Divigalpitiya, J. C. Irwin, and R. F. Frindt, Phys. Rev. B **43**, 12 053 (1991).

[20] S. M. Heald, D. L. Brewe, E. A. Stern, K. H. Kim, F. C. Brown, D. T. Jiang, E. D. Crozier, and R. A. Gordon, J. Synchrotron Radiat. **6**, 347 (1999); S. M. Heald, E. A. Stern, D. L. Brewe, R. A. Gordon, E. D. Crozier, D. T. Jiang, and J. O. Cross, *ibid.* **8**, 342 (2000).

[21] D. Yang and R. F. Frindt, J. Appl. Phys. **79**, 2376 (1996).

[22] M. Danot, J. L. Mansot, A. S. Golub, G. A. Protzenko, P. B. Fabritchnyi, Y. N. Novikov, and J. Rouxel, Mater. Res. Bull. **29**, 833 (1994).

[23] E. D. Crozier and A. J. Seary, Can. J. Phys. **59**, 876 (1981).

[24] S. I. Zabinsky, J. J. Rehr, A. Ankudinov, R. C. Albers, and M. J. Eller, Phys. Rev. B **52**, 2995 (1995).

[25] T. Ressler, J. Phys. IV **7**, C2-269 (1997).

[26] W. J. Schutte, J. L. De Boer, and F. Jellinek, J. Solid State Chem. **70**, 207 (1987).

[27] K. D. Bronsema, J. L. De Boer, and F. Jellinek, Z. Anorg. Allg. Chem. **540/541**, 15 (1986).